Engineered Science
DOI: https://dx.doi.org/10.30919/es1268

Development of Cupric Oxide/Porous Silicon (CuO/PS) Heterostructure Enabled Room Temperature Methane Sensor for Enhanced Industrial Safety

Khaniyev Bakyt,[1] Ibraimov Margulan,[1] Nalibayev Yerkebulan,[1] Skabylov Alisher,[1] Khaniyeva Ainur,[1] Jianxi Liu,[2] Tezekbay Yerbolat,[1] Duisebayev Tolagay,[1] Tileu Ayan[1] and Meirambekuly Nursultan[1,*]

Abstract

We report the development and characterization of a methane gas sensor made from copper oxide/porous silicon (CuO/PS) heterostructure. The sensor integrates the CuO layer on the PS surface, obtained by the DC magnetron sputtering technology, which increases the sensor's surface area and facilitates gas molecule interaction. We present an analysis of the sensor's morphological and structural characteristics, including detailed scanning electron microscopy (SEM) and X-ray diffraction (XRD) studies, and revealed the effective formation and interface of the heterostructure. The sensor demonstrates performance with good sensitivity to methane, characterized by a dynamic response. Sensitivity tests show a significant enhancement in signal response, and dynamic response evaluations indicate the repeatability of the sensor. The results suggest that the CuO/PS sensor offers a promising solution for methane detection, with potential applications in environmental monitoring, industrial safety, and process control.

Keywords: Methane gas sensor; Semiconductor heterostructure; Copper oxide; Porous silicon; Monitoring system; DC magnetron sputtering.
Received: 30 July 2024; Revised: 17 September 2024; Accepted: 18 September 2024.
Article type: Research article.

1. Introduction

Methane is a colorless and odorless gas that is used as fuel and raw materials in various industrial sectors.[1] However, methane leaks in large quantities pose serious risks.[2] Methane is highly flammable and can form explosive mixtures with air at concentrations from 4.9% to 15%. This makes methane leaks dangerous and potentially destructive.[3-7] In addition, methane leaks can pollute the air, soil and reservoirs, which can also have negative consequences for human health and ecosystems.[8,9] To minimize the risks associated with methane or other types of gases, it is extremely important to have effective systems for its detection.[10,11] Methane monitoring technologies and sensors, which can detect gas in low concentrations in real time, play a key role in ensuring safety at industrial facilities. These systems allow timely detection of leaks and prevention of their consequences, which helps to protect human health and maintain environmental balance.[11] The integration of reliable methane monitoring and detection systems is an essential component of industrial safety management. These systems help to prevent potential accidents, protect people and the environment, and ensure the safe operation of industrial facilities.[12-14]

Many studies have been conducted on methane detection, in which various approaches have been proposed, such as photonic crystal micro-cavity, hollow-core photonic band-gap fiber, surface plasmon resonance, utilization of the Vernier effect in fiber optic interferometers and spectroscopic methods.[15-18] Among all sensor technologies, optical and spectroscopic sensors are widely investigated.[19,20] Optical sensors for the detection of methane typically work by analysing the absorption of light at specific wavelengths that correspond to the absorption characteristics of methane. Zhang *et al*. developed an innovative optical methane sensor that integrates cryptophane-E into a photonic-crystal micro-cavity, combining the selective adsorption capabilities of cryptophane-E for methane with the high resonance

[1] *Department of Physics and Technology, Al-Farabi Kazakh National University, Al-Farabi av. 71, Almaty 050040, Kazakhstan.*
[2] *State Key Laboratory of Solidification Processing, Center of Advanced Lubrication and Seal Materials, School of Materials Science and Engineering, Northwestern Polytechnical University, Xi'an 710072, P.R. China.*
**Email:* nurs.kaznu@gmail.com (M. Nursultan)

characteristics of the photonic-crystal micro-cavity.[15] Martyniuk et al. reported on the Ga-free InAs/InAsSb type II superlattice (T2SL) based long wavelength infrared (LWIR) methane sensor operating at λ ~ 8 μm and capable of detecting methane at the ppb level in the LWIR region.[21] Yang *et al.* presented a photonic-crystal fiber methane sensor based on modal interference with a good sensitivity and a low detection limit.[22] However, the potential for widespread use of such sensors in practice is limited by the high cost and structural complexity of optical sensors, their high sensitivity to environmental conditions such as temperature and humidity, and their susceptibility to dust and other small particles that can affect the accuracy of methane detection. Therefore, it is necessary to find other methods or technologies for methane detection. One of these methods is the use of gas sensors based on metal oxide semiconductors (MOS) to detect methane.[23] MOS based gas sensors have several advantages that make them popular for various applications including methane detecting, as low cost, small size, high sensitivity, fast response time, and simplicity of manufacturing.[24-26] Many studies have been conducted to investigate the characteristics of methane sensors based on MOS, such as SnO_2, ZnO, TiO_2, Co_3O_4, and WO_3.[27-32]

One of the MOS materials with unique optical, electrical, and morphological properties that has a high potential for use in gas sensor technology is CuO.[33] CuO band gap is 1.2 eV, and it is characterized by p-type conductivity.[34] Kim *et al.* created interconnected p-CuO nanowires through thermal oxidation which can detect 10 ppm of NO_2 at an operating temperature in the range of 200 °C-400 °C.[35] Lai *et al.* fabricated a gas sensor using CuO nanowires on patterned interdigitated electrodes, which can detect ozone gas at a low concentration of 50 ppb at 100 °C.[36] The main drawbacks of MOS sensors include operating at high temperatures and poor compatibility with modern silicon-based electronic devices. In order to increase the sensitivity and reduce the operating temperature, CuO films with a porous structure and high surface activity can be prepared. Thus, through the deposition of CuO on a porous silicon (PS) surface and the formation of a heterostructure structure, it is possible to improve its sensing performance at room temperature. PS combines high specific surface area, chemical inertness, ease of integration with microelectronic systems and thermal stability, making it an ideal choice as a substrate for gas sensors. These properties ensure high sensitivity, reliability and durability of sensors, which is critical for their effective operation in various applications.[37,38] There have been some reports on the gas detection of PS/WO_3, PS/ZnO, PS/V_2O_5, PS/TeO_2 composites.[39-43] Nevertheless, the methane sensing properties of PS/CuO heterostructures have not been reported.

In this paper, the CuO/PS heterojunction structure and its optical, morphological, and sensing properties for methane detection are presented.

2. Experimental section

In this work the PS samples are used as substrates of the heterostructure material. The PS samples were produced through the electrochemical etching method, a widely used technique due to its effectiveness and relative simplicity. A porous layer was formed on the surface of a p-type silicon wafer, with an orientation and resistance of 10 Ohm·cm. To facilitate handling, the silicon wafer was cut into 1 × 1 cm^2 pieces (Fig. 1a). Before initiating the etching process, the silicon wafer was immersed in a hydrofluoric acid (HF) solution for 10 seconds to remove any impurities and then cleaned with ethanol to ensure a clean surface. The electrochemical etching was performed in a fluoroplastic Teflon cell using an electrolyte with a 1:1 volume ratio of HF and ethanol. The etching process was performed for 40 min with a stable current density of 5 mA/cm^2. The samples were then rinsed with deionized water and left to dry in the air. The porosity was determined using the gravimetric method (Fig. 1b).

The copper oxide (CuO) layer in the PS surface were prepared through magnetron sputtering followed by annealing. The magnetron sputtering process was carried out using the Kurt J. Lesker LAB-18 magnetron system. (Kurt J. Lesker Company, Dresden, Germany). A CuO target with a purity of

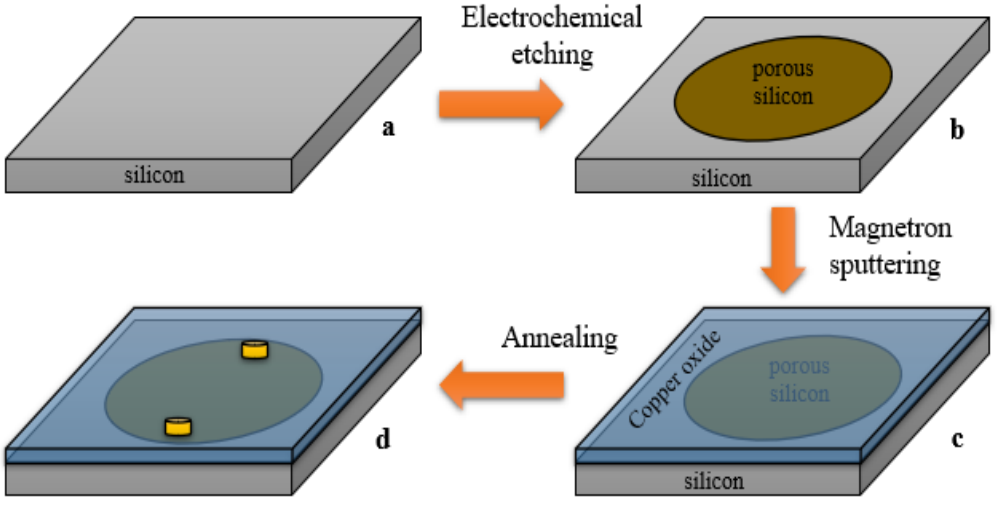

Fig. 1 Schematic illustration of the process for forming CuO/PS gas sensor.

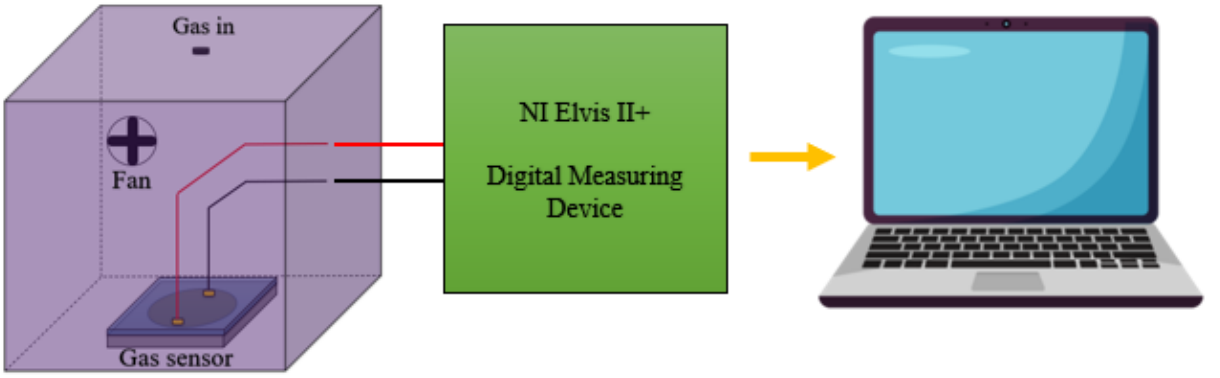

Fig. 2 Schematic diagram of the gas sensing measurement system.

99.999% was used to deposit the CuO layer in an atmosphere of argon (Ar) and oxygen (O_2). Ar and O_2 gases were introduced into the chamber in a ratio of 4:1. Deposition of the CuO layer on the PS samples was carried out for 30 min at power 100W, gas pressure 10.5 mTorr, and substrate-to-target distance of 13 cm. After the formation of CuO on the surface of the PS sample, the sample was kept in a furnace at a temperature of 650 °C for 4 h to crystallize (Fig. 1c).

The thickness of the CuO layer on the PS surface was measured using a profilometer Dektak XT Stylus profilometer (Bruker, Billerica, Massachusetts, USA). The morphology of the samples was analyzed using a scanning electron microscope JSM-IT2000 (JEOL Ltd., Tokyo, Japan). The XRD spectra, which were used to examine the phase formation of the samples, were acquired using a Rigaku Miniflex 600 diffractometer (Rigaku, Tokyo, Japan). Structural analysis was done by Raman spectroscopy using NT-MDT Solver Spectrum with a laser excitation wavelength of 473 nm.

Two ohmic contacts of InGa alloy were deposited on the surface of the samples in a coplanar configuration using thermal deposition to measure their electrical characteristics (Fig. 1d). The gas sensing measurement was carried out at room temperature using a chamber with a volume of 8L (Fig. 2). The base gas in the measurement is pure air. The current-voltage characteristics and sensing response curves were measured with NI Elvis II+ module.

3. Results and discussion

The morphology of the PS and the CuO/PS samples were observed from the scanning electron microscopy (SEM) images, which are shown in Fig. 3. The SEM image of the PS sample reveals a highly textured surface characterized by numerous interconnected pore-like structures (Fig. 3a). The surface is predominantly covered with an intricate network of pores, varying in size and shape. These pores are distributed uniformly across the surface, giving the material a sponge-like appearance. The porosity value was 72%. The cross-section view of the PS shows aligned channels. Fig. 3b shows the surface of the CuO layer deposited on PS, revealing a uniform porous structure, so high porosity, large specific surface area as well as diffusion conduits for gas molecules can be achieved. The thickness of the CuO layer was measured by using a profiler and amounted to 132 nm.

The structure of the CuO/PS sample was characterized using XRD and Raman spectroscopy (Fig. 4). The Raman spectrum of the CuO/PS sample shows typical characteristic

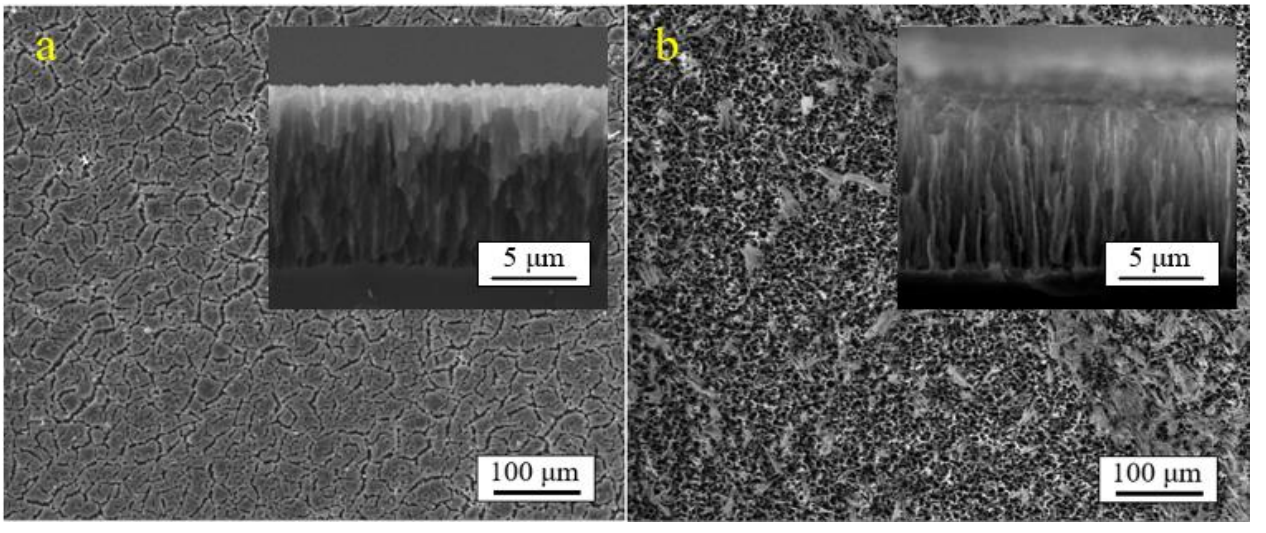

Fig. 3 Top-view and cross-sectional SEM images of the PS (a) and the CuO/PS (b) samples.

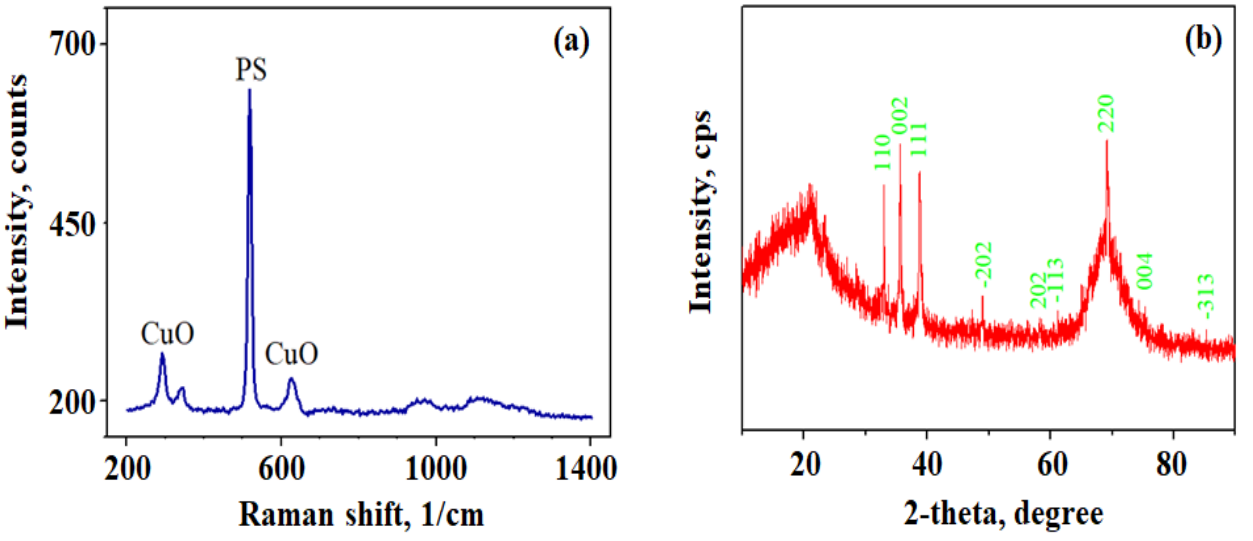

Fig. 4 Raman spectrum (a) and XRD pattern (b) of the CuO/PS sample.

peaks associated with both CuO and the PS substrate (Fig. 4a). For CuO, prominent peaks corresponding to the bending and stretching vibrations of the Cu-O bonds are observed, particularly around 300 cm^{-1} and 620 cm^{-1}, indicative of the presence of CuO in its different phases.[44] In addition, the PS component contributes a peak around 520 cm^{-1}, associated with the Si–Si bond vibrations.[45]

The XRD pattern of the CuO/PS heterostructure reveals distinct diffraction peaks corresponding to the crystalline phases of CuO and PS. Peaks typically observed for CuO include those at 2θ values of approximately 35.6°, 38.7°, 48.8°, and 61.5°, corresponding to the (110), (111), (202), and (220) planes of the monoclinic CuO phase, respectively. A sharp diffraction peak can be seen at 69.2° for the as-prepared PS sample, corresponding to the plane reflection of Si.[46] Additionally, there is a broad hump in the region of 15–30° and it is likely related to the formation of an amorphous SiO_2 phase.[47] The strong diffraction peaks of CuO appear at 35.662°, 38.853°, and 48.954°, corresponding to the (110), (111), and (202) planes of the monoclinic CuO phase, respectively.[48] These peaks confirm the presence and crystalline nature of CuO within the heterostructure. The values match precisely with the standard data (PDF Card No.: 00-041-0254).

Figure 5 depicts the current-voltage characteristics of the CuO/PS sample measured under the influence of 10 ppm methane and in air at room temperature. In air, the current-voltage curve exhibits a baseline behavior where the current changes predictably with applied voltage, showing a quiet linear relationship. When exposed to methane with a concentration of 10 ppm, the current-voltage characteristics changed, reflecting the sample's response to the gas. One might observe an increase in current due to the interaction between methane molecules and the sample's surface, which can alter its electrical conductivity. This increase in current may be due to enhanced charge carrier activity or changes in the sample's electronic structure caused by the gas interaction. It was determined that the sensor current reaches saturation at a certain concentration of methane gas. Therefore, the CuO/PS gas sensor has an upper limit of gas concentration at which the current value is saturated.

Figure 6 shows the dynamic response curve of the CuO/PS sample when exposed to methane at a concentration of 10 ppm at room temperature. It can be seen that the current increases dramatically upon exposure to methane and recovers after clean air flows into the chamber. The response/recovery time of the sensor can be determined from the dynamic response of the sensor and amounted to 20 sec and 100 sec, respectively, which are similar with other researches.

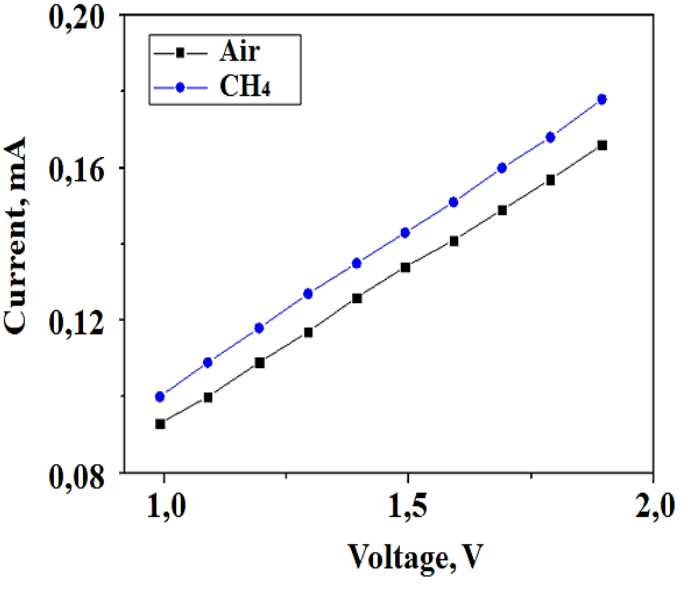

Fig. 5 The current-voltage characteristics of the CuO/PS sample under the influence of 10 ppm methane and in air.

Measurements showed that the sensor response of the CuO/PS sensor to methane gas reaches 7%. The sensor response of the sensor was calculated as:[49]

$$S_R = \frac{I_{gas} - I_{air}}{I_{air}} \quad (1)$$

where I_{air} and I_{gas} are the currents (resistances) measured in the air and target gas (methane) ambiences, respectively.

An energy band diagram can be used to explain the sensing mechanism of the CuO/PS sample. The band gap of PS is larger than that of silicon due to the quantum confinement effect.[50] The electronic affinity of PS is similar with Si (4.01 eV). As for CuO, also an p-type semiconductor, Eg (CuO) = 1.35 eV, χ(CuO) = 4.07 eV.[51] When these two semiconductors come into contact with each other, a p-n heterostructure is formed at the interface. Due to the difference in Fermi energies, electrons from CuO with higher energies flow from CuO to PS, while holes flow in the opposite direction until the Fermi levels become equal. This results in a depletion layer on the PS side and a hole accumulation layer on the CuO side. Due to the different dielectric constants of CuO and PS, the energy bands become discontinuous. This efficient charge separation results from the heterostructure, which offers a high concentration of charge carriers in the accumulation layer, increasing the lifetime of these carriers. Consequently, the material facilitates easier exchange of electrons with adsorbed gases.

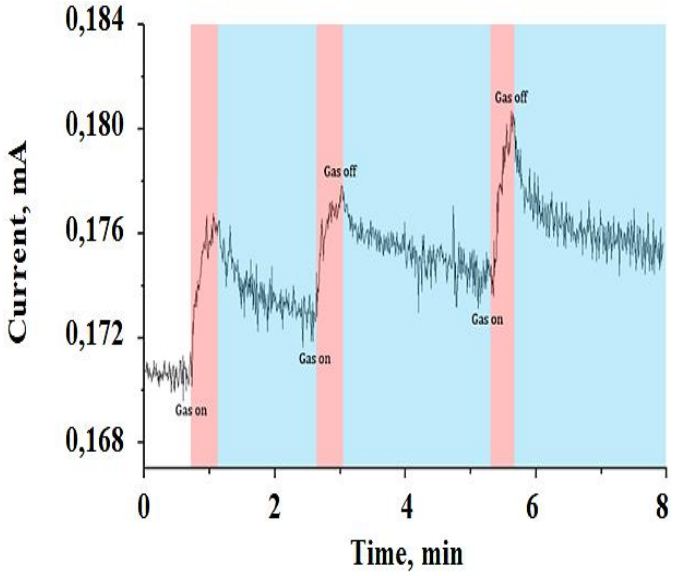

Fig. 6 The dynamic response of the CuO/PS sample to methane.

When the sensor is exposed to air, oxygen molecules are adsorbed onto its surface. Due to the sensor's large specific surface area, it offers numerous active sites for gas adsorption. This extensive surface area increases the number of active centers available for oxygen molecule attachment. Consequently, a larger specific surface area results in a higher density of oxygen vacancies on the material's surface. As a result, the sensor can adsorb a significant number of oxygen molecules even at room temperature. Oxygen molecules adsorbed on the surface exchange with electrons on the sensor surface to form oxygen ions O_2^- which are stable at the working room temperature. As a result, the energy band of the CuO/PS heterostructure becomes further bent. When gas molecules interact with the sensor, an acidification reaction occurs between the gas molecules and oxygen anions. This reaction increases the concentration of defects in the accumulation layer and reduces the sensor's resistance.

4. Conclusions

In conclusion, this work demonstrates the promising potential of the methane gas sensor prepared using CuO/PS heterostructure. Through detailed analysis of the morphological and structural characteristics, the heterostructure's unique interface significantly enhances the sensor's functional properties was established. The intricate morphology of the PS and the well-defined structure of the CuO layer contribute to the effective interaction with methane gas molecules, leading to improved sensitivity. The sensor exhibits notable sensitivity (7%) and dynamic response to methane at room temperature. The gas sensing mechanism was explained using the energy band diagram and was attributed to the synergistic effects of CuO and PS materials, which facilitate efficient charge transfer and enhance gas adsorption.

Our findings suggest that this sensor architecture not only provides a reliable and efficient means for methane detection but also paves the way for further advancements in gas sensing technology. Future research will focus on further optimization of the sensor's material composition and structure, as well as exploring its long-term stability, selectivity and performance in diverse environments. The insights gained from this study provide a solid foundation for developing advanced methane sensors with improved accuracy and reliability, with potential implications for environmental monitoring, safety, and industrial applications.

Acknowledgements

This research was funded by the Science Committee of the Ministry of Science and Higher Education (MHES) of the Republic of Kazakhstan under Grant No. AP19678266.

Conflict of Interest

There is no conflict of interest.

Supporting Information

Not applicable.

References

[1] L. F. Mullagaliyeva, S. K. Baimukhametov, V. S. Portnov, V. M. Yurov, On the issue of thermal destruction of coal matter, *Engineering Journal of Satbayev University*, 2022, **144**, 57-61, doi: 10.51301/ejsu.2022.i1.09.

[2] M. Li, X. Sun, Y. Wang, C. Qin, J. Cao, Y. Wang, Light-driven room temperature methane gas sensor based on Ag modified flower-like ZnO microsphere, *Sensors & Diagnostics*, 2023, **2**, 878-886, doi: 10.1039/D3SD00068K.

[3] I. V. Sedov, V. S. Arutyunov, M. V. Tsvetkov, D. N. Podlesniy, M. V. Salganskaya, A. Y. Zaichenko, Y. Y. Tsvetkova, A. V. Nikitin, A. V. Ozerskii, I. G. Fokin, E. A. Salgansky, Evaluation

of the possibility to use coalbed methane to produce methanol both by direct partial oxidation and from synthesis gas, *Eurasian Chemico-Technological Journal*, 2022, **24**, 157, doi: 10.18321/ectj1328.
[4] G. Y. Yergaziyeva, E. Kutelia, K. Dossumov, D. Gventsadze, N. Jalabadze, T. Dzigrashvili, L. Nadaraia, O. Tsurtsumia, M. M. Anissova, M. M. Mambetova, B. Eristavi, N. Khudaibergenov, Effect of lanthanum oxide on the activity Ni-co/diatomite catalysts in dry reforming of methane, *Eurasian Chemico-Technological Journal*, 2023, **25**, 21-32, doi: 10.18321/ectj1492.
[5] E. V. Matus, M. A. Kerzhentsev, A. P. Nikitin, S. A. Sozinov, Z. R. Ismagilov, Promising directions in chemical processing of methane from coal industry. part 3. catalytic tests, *Eurasian Chemico-Technological Journal*, 2024, **26**, 3-14, doi: 10.18321/ectj1559.
[6] E. V. Matus, M. A. Kerzhentsev, A. P. Nikitin, S. A. Sozinov, Z. R. Ismagilov, Promising directions in chemical processing of methane from coal industry. part 2. development of catalysts, *Eurasian Chemico-Technological Journal*, 2023, **25**, 103-113, doi: 10.18321/ectj1500.
[7] S. N. Longinos, D. D. Longinou, E. Celebi, Z. Toktarbay, M. Parlaktuna, Kinetic study of methane hydrate formation with the use of a surface baffle, *Reaction Kinetics, Mechanisms and Catalysis*, 2021, **134**, 75-86, doi: 10.1007/s11144-021-02058-w.
[8] S. N. Longinos, D. D. Longinou, N. Myrzakhmetova, N. Akimbayeva, M. Zhursumbaeva, K. Abdiyev, Z. Toktarbay, M. Parlaktuna, Kinetic analysis of methane hydrate formation with butterfly turbine impellers, *Molecules*, 2022, **27**, 4388, doi: 10.3390/molecules27144388.
[9] L. Han, S. Zhang, B. Zhang, B. Zhang, Y. Wang, H. Bala, Z. Zhang, Dual-selective detection of CO and CH_4 based on hierarchical porous In_2O_3 nanoflowers with Pd modification, *Journal of Materiomics*, 2022, **8**, 545-555, doi: 10.1016/j.jmat.2021.12.006.
[10] J. Dai, G. Xie, C. Chen, Y. Liu, H. Tai, Y. J., Y. Su, Hierarchical piezoelectric composite film for self-powered moisture detection and wearable biomonitoring, *Applied Physics Letters*, 2024, **124**, 053701, doi: 10.1063/5.0187539.
[11] Y. Li, W. Li, Z. Jin, X. Luo, G. Xie, H. Tai, Y. Jiang, Y. Yang, Y. Su, Ternary ordered assembled piezoelectric composite for self-powered ammonia detection, *Nano Energy*, 2024, **122**, 109291, doi: 10.1016/j.nanoen.2024.109291.
[12] Z. Darynova, B. Blanco, C. Juery, L. Donnat, O. Duclaux, Data assimilation method for quantifying controlled methane releases using a drone and ground-sensors, *Atmospheric Environment: X*, 2023, **17**, 100210, doi : 10.1016/j.aeaoa.2023.100210.
[13] H. Wang, W. Zhang, C. Chen, S. Tang, H. Liu, A new methane sensor based on compound film-coated photonic crystal fiber and Sagnac interferometer with higher sensitivity, *Results in Physics*, 2019, **15**, 102817, doi: 10.1016/j.rinp.2019.102817.
[14] Y. Su, S. Chen, B. Liu, H. Lu, X. Luo, C. Chen, W. Li, Y. Long, H. Tai, G. Xie, Y. Jiang, Maxwell displacement current induced wireless self-powered gas sensor array, *Materials Today Physics*, 2023, **30**, 100951, doi: 10.1016/j.mtphys.2022.100951.
[15] C. Chen, G. Xie, J. Dai, W. Li, Y. Cai, J. Li, Q. Zhang, H. Tai, Y. Jiang, Y. Su, Integrated core-shell structured smart textiles for active NO2 concentration and pressure monitoring, *Nano Energy*, 2023, **116**, 108788, doi: 10.1016/j.nanoen.2023.108788.
[16] Y. N. Zhang, Y. Zhao, Q. Wang, Measurement of methane concentration with cryptophane E infiltrated photonic crystal microcavity, *Sensors and Actuators B: Chemical*, 2015, **209**, 431-437, doi: 10.1016/j.snb.2014.12.002.
[17] Z. F. Wu, C. T. Zheng, Z. W. Liu, D. Yao, W. X. Zheng, Y. D. Wang, F. Wang, D. M. Zhang, Investigation of A slow-light enhanced near-infrared absorption spectroscopic gas sensor, based on hollow-core photonic band-gap fiber, *Sensors*, 2018, **18**, 2192, doi: 10.3390/s18072192.
[18] H. Liu, M. Wang, Q. Wang, H. Li, Y. Ding, C. Zhu, Simultaneous measurement of hydrogen and methane based on PCF-SPR structure with compound film-coated side-holes, *Optical Fiber Technology*, 2018, **45**, 1-7, doi: 10.1016/j.yofte.2018.05.007.
[19] Y. Li, H. Chen, H. Li, C. Liu, J. Li, Q. Chen, K. Li, S. Zhang, M. Gu, Ultra-high sensitivity methane gas sensor based on vernier effect in double D-shaped and cryptophane-A film-coated photonic crystal fiber: Design and FEM simulation, *Results in Physics*, 2023, **52**, 106840, doi: 10.1016/j.rinp.2023.106840.
[20] T. Aldhafeeri, M. K. Tran, R. Vrolyk, M. Pope, M. Fowler, A Review of Methane Gas Detection Sensors: Recent Developments and Future Perspectives, *Inventions*, 2020, **5**, 28, doi: 10.3390/inventions5030028.
[21] N. M. Davis, D. Francis, J. Hodgkinson, R. P. Tatam, Compact methane sensor using an integrating sphere and interband cascade laser at 3313nm, *Sensors and Actuators B: Chemical*, 2023, **389**, 133866, doi: 10.1016/j.snb.2023.133866.
[22] P. Martyniuk, J. Wojtas, K. Michalczewski, W. Gawron, J. Mikołajczyk, S. Krishna, Demonstration of the long wavelength InAs/InAsSb type-II superlattice based methane sensor, *Sensors and Actuators A: Physical*, 2021, **332**, 113107, doi: 10.1016/j.sna.2021.113107.
[23] J. Yang, L. Zhou, X. Che, J. Huang, X. Li, W. Chen, Photonic crystal fiber methane sensor based on modal interference with an ultraviolet curable fluoro-siloxane nano-film incorporating cryptophane A, *Sensors and Actuators B: Chemical*, 2016, **235**, 717-722, doi: 10.1016/j.snb.2016.05.125.
[24] M. Bagheri, A. Ali Khodadadi, A. R. Mahjoub, Y. Mortazavi, Strong effects of Gallia on structure and selective responses of Ga_2O_3–In_2O_3 nanocomposite sensors to either ethanol, CO or CH_4, *Sensors and Actuators B: Chemical*, 2015, **220**, 590-599, doi: 10.1016/j.snb.2015.06.007.
[25] S. Khasim, A. Pasha, N. Badi, A. Ltaief, S. A. Al-Ghamdi, C. Panneerselvam, Design and development of highly sensitive PEDOT-PSS/AuNP hybrid nanocomposite-based sensor towards room temperature detection of greenhouse methane gas at ppb level, *RSC Advances*, 2021, **11**, 15017-15029, doi: 10.1039/d1ra00994j.
[26] D. Xue, P. Wang, Z. Zhang, Y. Wang Chemical, Enhanced methane sensing property of flower-like SnO2 doped by Pt nanoparticles: A combined experimental and first-principle study,

Sensors and Actuators B: Chemical, 2019, **296**, 126710, doi: 10.1016/j.snb.2019.126710.
[27] M. Bai, R. Chen, X. Liu, H. Li, J. Li, H. Huang, M. Song, Q. Zhang, Y. Su, H. Wang, M. Xu, G. Xie, An effective strategy for synthesizing high-performance photocatalyst by recycling the graphite target wastes, *Journal of Environmental Chemical Engineering*, 2024, **12**, 113872, doi: 10.1016/j.jece.2024.113872.
[28] Q. Zhang, G. Xie, M. Duan, Y. Liu, Y. Cai, M. Xu, K. Zhao, H. Tai, Y. Jiang, Y. Su, Zinc oxide nanorods for light-activated gas sensing and photocatalytic applications, *ACS Applied Nano Materials*, 2023, **6**, 19, 17445-17456, doi: 10.1021/acsanm.3c02403.
[29] L. Yang, Z. Wang, X. Zhou, X. Wu, N. Han, Y. Chen, Synthesis of Pd-loaded mesoporous SnO2 hollow spheres for highly sensitive and stable methane gas sensors, *RSC Advances*, 2018, **8**, 24268–24275, doi: 10.1039/C8RA03242D.
[30] S. Zhang, Y. Li, G. Sun, Bo Zhang, Y. Wang, J. Cao, Z. Zhang, Synthesis of NiO-decorated ZnO porous nanosheets with improved CH_4 sensing performance, *Applied Surface Science*, 2019, **497**, 143811, doi: 10.1016/j.apsusc.2019.143811.
[31] Z. P. Tshabalala, H. C. Swart, D. E. Motaung, Fabrication of TiO_2 nanofibers-based sensors for enhanced CH_4 performance induced by notable surface area and acid treatment, *Vacuum*, 2021, **187**, 110102, doi: 10.1016/j.vacuum.2021.110102.
[32] N. M. Shaalan, M. Rashad, A. H. Moharram, M. A. Abdel-Rahim, Promising methane gas sensor synthesized by microwave-assisted Co_3O_4 nanoparticles, *Materials Science in Semiconductor Processing*, 2016, **46**, 1-5, doi: 10.1016/j.mssp.2016.01.020.
[33] D. Xue, J. Wang, Y. Wang, G. Sun, J. Cao, H. Bala, Z. Zhang, Enhanced methane sensing properties of WO_3 nanosheets with dominant exposed (200) facet via loading of SnO_2 nanoparticles, *Nanomaterials*, 2019, **9**, 351, doi: 10.3390/nano9030351.
[34] B. Khaniyev, M. Ibraimov, Y. Sagidolda, Y. Tezekbay, T. Duisebayev, A. Tileu, A. Khaniyeva, The improved non-polar gas sensing performance of surface-modified porous silicon-based gas sensors, *Coatings*, 2023, **13**, 190, doi: 10.3390/coatings13010190.
[35] B. Chakraborty, D. Litra, A.K. Mishra, C. Lupan, R. Nagpal, S. Mishra, H. Qiu, S. Railean, O. Lupan, N.H. de Leeuw, R. Adelung, L. Siebert, Multistep Synthesis, Growth mechanism, optical, and microwave absorption properties of ZnO dendritic nanostructures, *Journal of Alloys and Compounds*, 2024, **1002**, 175385, doi: 10.1016/j.jallcom.2024.175385.
[36] J. H. Kim, A. Katoch, S. W. Choi, S. S. Kim, Growth and sensing properties of networked p-CuO nanowires, *Sensors and Actuators B: Chemical*, 2015, **212**, 190-195, doi: 10.1016/j.snb.2014.12.081.
[37] L. T. Lai, H. T. Hsueh, C. H. Chiu, T. C. Cheng, S. J. Chang, Thermal oxidation CuO nanowire gas sensor for ozone detection applications, *Sensors and Actuators Reports*, 2024, **8**, 100228, doi: 10.1016/j.snr.2024.100228.
[38] B. A. Khaniyev, Y. Sagidolda, K. K. Dikhanbayev, A. O. Tileu, M. K. Ibraimov, High sensitive NH_3 sensor based on electrochemically etched porous silicon, *Cogent Engineering*, 2020, **7**, 1810880, doi: 10.1080/23311916.2020.1810880.
[39] M. K. Ibraimov, Y. Sagidolda, S. L. Rumyantsev, Z. Z. Zhanabaev, M. S. Shur, Selective gas sensor using porous silicon, *Sensor Letters*, 2016, **14**, 588-591, doi: 10.1166/sl.2016.3657.
[40] P. Zeng, P. Zhang, M. Hu, S.-Y. Ma, W.-J. Yan, Synthesis and room-temperature NO_2 gas sensing properties of a WO_3 nanowires/porous silicon hybrid structure, *Chinese Physics B*, 2014, **23**, 058103, doi: 10.1088/1674-1056/23/5/058103.
[41] D. Yan, M. Hu, S. Li, J. Liang, Y. Wu, S. Ma, Electrochemical deposition of ZnO nanostructures onto porous silicon and their enhanced gas sensing to NO2 at room temperature, *Electrochimica Acta*, 2014, **115**, 297-305, doi: 10.1016/j.electacta.2013.10.007.
[42] W. Yan, M. Hu, D. Wang, C. Li, Room temperature gas sensing properties of porous silicon/V_2O_5 nanorods composite, *Applied Surface Science*, 2015, **346**, 216-222, doi: 10.1016/j.apsusc.2015.01.020.
[43] J. H. Bang, M. S. Choi, A. Mirzaei, S. Han, H. Y. Lee, S. W. Choi, S. S. Kim, H. W. Kim, Hybridization of silicon nanowires with TeO_2 branch structures and Pt nanoparticles for highly sensitive and selective toluene sensing, *Applied Surface Science*, 2020, **525**, 146620, doi: 10.1016/j.apsusc.2020.146620.
[44] L.V. A. Sayson, M. L. Joybelle, S. E. Elmer, A. S. Arnel, S. S. Armando, Nanostructured CuO thin film deposited on stainless steel using spray pyrolysis as supercapacitor electrode, *Materials Research Express*, 2020, **6**, 125551, doi: 10.1088/2053-1591/ab6921.
[45] R. Venkatesan, J. Mayandi, J. M. Pearce, V. Venkatachalapathy, Influence of metal assisted chemical etching time period on mesoporous structure in as-cut upgraded metallurgical grade silicon for solar cell application, *Journal of Materials Science: Materials in Electronics*, 2019, **30**, 8676-8685, doi: 10.1007/s10854-019-01191-6.
[46] F. A. Harraz, A. A. Ismail, S. A. Al-Sayari, A. Al-Hajry, M. S. Al-Assiri, A highly sensitive and durable electrical sensor for liquid ethanol using thermally-oxidized mesoporous silicon, *Superlattices and Microstructures*, 2016, **100**, 1064-1072, doi: 10.1016/j.spmi.2016.10.074.
[47] A. M. S. Salem, F. A. Harraz, S. M. El-Sheikh, H. S. Hafez, I. A. Ibrahim, M. S. A. Abdel-Mottaleb, Enhanced electrical and luminescent performance of a porous silicon/MEH-PPV nanohybrid synthesized by anodization and repeated spin coating, *RSC Advances*, 2015, **5**, 99892-99898, doi: 10.1039/c5ra18407j.
[48] X. Liu, M. Hu, Y. Wang, J. Liu, Y. Qin, High sensitivity NO_2 sensor based on CuO/p-porous silicon heterojunction at room temperature, *Journal of Alloys and Compounds*, 2016, **685**, 364–369, doi: 10.1016/j.jallcom.2016.05.215.
[49] I. P. Liu, C. H. Chang, T. C. Chou, K. W. Lin, Ammonia sensing performance of a platinum nanoparticle-decorated tungsten trioxide gas sensor, *Sensors and Actuators B: Chemical*, 2019, **291**, 148-154, doi: 10.1016/j.snb.2019.04.046.
[50] J. Kanungo, H. Saha, S. Basu, Pd sensitized porous silicon hydrogen sensor—influence of ZnO thin film, *Sensors and*

Actuators B: Chemical, 2010, **147**, 128-136, doi: 10.1016/j.snb.2010.03.044.
[51] N. Datta, N. S. Ramgir, S. Kumar, P. Veerender, M. Kaur, S. Kailasaganapathi, A. K. Debnath, D. K. Aswal, S. K. Gupta, Role of various interfaces of CuO/ZnO random nanowire networks in H_2S sensing: an impedance and Kelvin probe analysis, *Sensors and Actuators B: Chemical*, 2014, **202**, 1270-1280, doi: 10.1016/j.snb.2014.06.072.

